INTERNATIONAL JOURNAL OF CLIMATOLOGY
Int. J. Climatol. (2017)
Published online in Wiley Online Library
(wileyonlinelibrary.com) DOI: 10.1002/joc.5307

RMetS
Royal Meteorological Society

Predictability of late-season tropical cyclone accumulated kinetic energy around Taiwan 2 months ahead

Mong-Ming Lu,[a]* Ching-Teng Lee[a] and Bin Wang[b,c]

[a] *Central Weather Bureau, Taipei, Taiwan*
[b] *Department of Atmospheric Sciences, Atmosphere-Ocean Research Center, University of Hawaii at Manoa, Honolulu, HI, USA*
[c] *Earth System Modeling Center, Nanjing University of Information Science and Technology, Nanjing, China*

ABSTRACT: Long-lead seasonal forecast of tropical cyclone (TC) activity is strongly demanded, albeit challenging, for hazard prevention and preparedness in the area prone to TCs. This article attempts to present a late-season (September–November, SON) empirical prediction model to predict the accumulative cyclone kinetic energy (ACE) around Taiwan. The predictors are the sea-surface temperatures (SSTs) and sea-level pressure (SLP) anomaly during the preceding spring and summer seasons over tropical Southeast Asia, subtropical western and central North Pacific, and subtropical North Atlantic. Three prediction models are established with the lead times of 0, 1, and 2 months. Different types of large-scale influence on the TC activity are found for the above and below-normal-ACE years, respectively. For the above-normal-ACE years, the favourable large-scale condition is warm SSTs over the west Pacific, South China Sea (SCS), and eastern Indian Ocean, and the associated anomalous cyclonic winds and low SLP over the west Pacific marginal seas. The robust precursors are the warm SSTs over mid-latitude west North Pacific and North Atlantic, and the low SLP over Atlantic during the preceding spring season. For the below-normal-ACE years, the favourable large-scale condition is cold SSTs over Indonesian seas and equatorial west Pacific, warm SST and low SLP over equatorial east Pacific, and the anomalous anticyclonic circulation over the SCS and the Philippine Sea. The robust precursors are the anomalous SST and SLP during the preceding spring season, with the opposite signs to the above-normal-ACE years. The presented models built on the precursor signals are proved able to generate skilful forecast 2 months ahead. The product ACE-SON can be used for seasonal TC activity outlook in a larger area including the coastal region of southeast China and for seasonal rainfall outlook in Taiwan.

KEY WORDS tropical cyclone predictability; western North Pacific typhoons; seasonal forecast; empirical prediction model; Southeast Asia climate; Taiwan climate

Received 18 May 2017; Revised 4 August 2017; Accepted 8 September 2017

1. Introduction

Tropical cyclone (TC) is the most influential high-impact weather system to Taiwan. About 50% of annual total rainfall amount and 80% of weather-related losses and damage in Taiwan are associated with TC activity. Suffice it to say that accurate TC prediction for the time range from hours to months in advance is of extreme importance to the safety and wellbeing of the 23 million residents on Taiwan island. The focus of this study is on investigating the predictability of long-lead prediction of the TC activity around Taiwan.

Taiwan is located in a region that prone to TC Passage. The TC density maps over the western North Pacific (WNP) shown in Figures 1(a) and (b) for June–August (JJA) and September–November (SON), respectively, clearly present that Taiwan is embedded in the area with highest TC density particularly during the JJA season. The TC density here is calculated at each 2.5° by degree latitude and longitude pixel represented in percentage that is based on the 46-year (1970–2015) total count of the TCs detected at the pixel divided by the sum of the counts of all pixels in domain. The TC affecting Taiwan is defined as the TC centre entered an area with the boundary as Taiwan's coastline expanded outwards by 300 km on a $0.1 \times 0.1°$ of latitude and longitude mesh (Figure 1; Lu *et al.*, 2013, hereinafter referred to as LLW). Figures 1(c) and (d) are the density maps of the affecting Taiwan TCs with entire life taken into account. The JJA map (Figure 1(c)) shows higher TC density over the South China Sea (SCS) than the SON (Figure 1(d)) whereas the SON map shows higher density over northern Philippines than the JJA. The difference between SON and JJA densities (Figure 1(e)) is southeast–northwest oriented tails with higher TC density in SON from Pacific to the Philippine Sea. It suggests that although less frequent the SON TCs have higher possibility of travelling a longer distance over the ocean before invading Taiwan, which is higher than that for JJA TCs. In fact, TC damage in SON on average is more serious than that in JJA.

In this study, the predictand is the accumulative cyclone kinetic energy (ACE) of the affecting Taiwan TCs. Slightly

* Correspondence to: M.-M. Lu, Central Weather Bureau, No. 64, Gongyuan Road, Taipei 10048, Taiwan.
E-mail: mongminglu@gmail.com

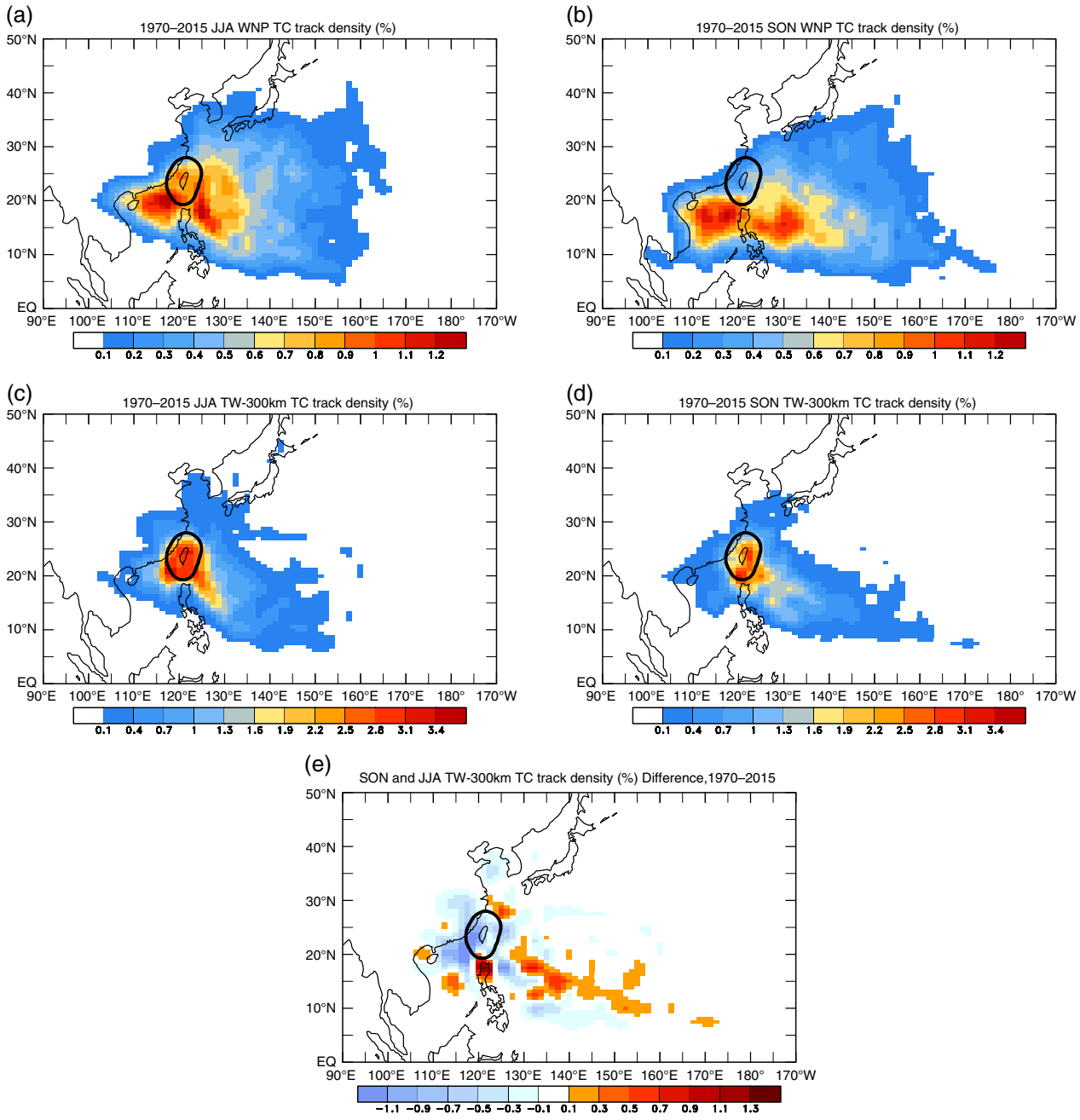

Figure 1. The TC track density map based on 6-h JTWC best track data from 1970 to 2015. The density is calculated in every 2.5 × 2.5° grid box as the total TC frequency in a box divided by the total TC frequency all over the entire WNP basin (equator 60°N, 180–100°E) accumulated over 3 months such as (a) June–July–August and (b) September–October–November, and the track density based on affecting Taiwan TCs for (c) JJA, (d), SON, and (e) the difference between SON and JJA. The black circle surround Taiwan represents the 300-km boundary when a TC centre moves across the boundary is affecting Taiwan. [Colour figure can be viewed at wileyonlinelibrary.com].

different from the ACE that used to measure the activity of individual TC and entire TC seasons, particularly, the Atlantic tropical seasons (Bell *et al.*, 2000), the ACE of the present article refers to the sum of the squares of the maximum sustained surface wind speed (knots) measured every 6 h when the TC is within the influence domain and only the named system counted. Note that a named system's intensity must reach at least tropical storm strength (wind speed $\geq 34\,\mathrm{kt\,h^{-1}}$) during the storm's entire lifetime. The ACE seasonal distribution (Figure 2) shows that 61% of the annual ACE contributed by the 'invading' TCs before September. Table 1 shows the ACE correlation between different seasons. The correlation is very low between two successive seasons when there is no overlapped month(s). For the TC peak season (JJAS), an ACE forecast model presented in LLW is used at the Central Weather Bureau (CWB) of Taiwan for real-time forecast. However, for the late season (SON) there is not yet a forecast model available. The purpose of this study is to build a SON ACE forecast model for Taiwan area and to identify the sources of the predictability.

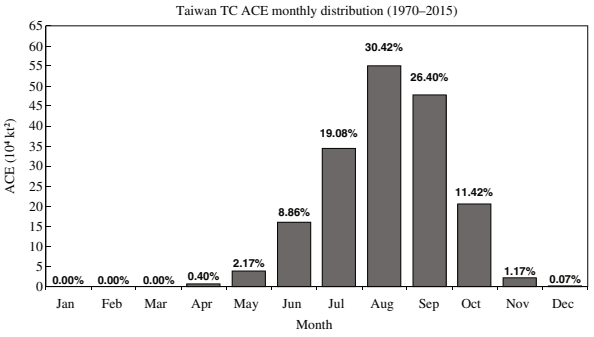

Figure 2. The 1970–2015 climate mean monthly ACE of the affecting Taiwan TC and its percentage with relative to the annual total ACE.

Table 1. The correlation of the ACE of affecting Taiwan TC between different seasons during 1970–2007.

	AMJ	MJJ	JJA	JAS	ASO	SON
AMJ	1	0.49	0.28	−0.1	−0.07	−0.12
MJJ	–	1	0.61	0.49	0.11	0.11
JJA	–	–	1	0.72	0.61	0.04
JAS	–	–	–	1	0.83	0.58
ASO	–	–	–	–	1	0.70
SON	–	–	–	–	–	1

AMJ, April–May–June; MJJ, May–June–July; JAS, July–August–September.

The layout of the article is as follows: Section 2 describes the data used in this study. The forecast model and skill evaluation are described in Section 3. The predictability and attribution analysis is presented in Section 4. Section 5 is discussion and application.

2. Data

The Joint Typhoon Warning Center (JTWC) best-track data set, available at 6-h sampling frequency over the period of 1970–2015, obtained from the website (http://metocph.nmci.navy.mil/jtwc/best_tracks/), was used to calculate the ACE. TC refers to tropical storms and typhoons, which has a maximum sustained surface wind speed of 33 m s^{-1} or higher. The wind speed estimation of an individual typhoon is sensitive to the size and area integration (Yu *et al.*, 2009). The sensitivity is less important for seasonal forecast.

The large-scale environment data used for deriving the predictors are the National Centers for Environmental Prediction (NCEP)-National Center for Atmospheric Research (NCAR) reanalysis data set (Kalnay *et al.*, 1996) and the extended reconstructed sea-surface temperature (ERSST) data set prepared by the National Climate Data Center (NCDC), downloaded from the NOAA Physical System Division of the Earth System Research Laboratory in Boulder website (http://www.cdc.noaa.gov/). The variables include global mean sea level pressure (MSLP), the 2-m temperature (T2m) over land, wind at 850 hPa (UV850), and sea-surface temperature (SST). The predictors are selected from the monthly data from March to August of these variables.

3. Forecast model and skill evaluation

3.1. Predictor selection procedure

As mentioned before, the predictand of the forecast model is the ACE in the 300-km area surrounding Taiwan accumulated during the late typhoon season (SON) denoted as ACE-SON. The predictors were selected using a two-step correlation analysis procedure. The first step is to calculate the correlation maps between ACE-SON and the large-scale environment variables in the latitudinal belt of 40°S–60°N. The area means of the variables and their derivatives showing high correlation with the predictand are chosen as the predictor candidates. The second step is to build the prediction models by selecting predictors from the candidates through a stepwise multivariate regression procedure. The confidence level of the prediction model is determined through the F-test.

The data during the years of 1970–2007 are used for building the forecast model including model forecast skill evaluation following the standard cross-validation procedures, while the years of 2008–2015 are used for forecast experiment that mimics the real-time forecast in the operational mode. The forecast performance during the experimental period of 2008–2015 is compared with the cross-validation result to evaluate the assessed forecast skill.

Following the same procedure as in LLW, the large-scale variables: sea-level pressure (SLP), SST, and 850-hPa winds (U850 and V850) are analysed to select the best predictors. The simultaneous and one-season lag correlation of ACE-SON and the large-scale variables are presented in Figures 3(a) and (b). The SST correlation pattern in Figure 3(a) resembles a La Niña-like pattern that shows clear SST contrast between the equatorial west and east Pacific (EP). Over the Pacific the inter-hemispheric low-level convergent flow is stronger over the eastern than the western margins. The subtropical eastern Pacific around 10°–20°N even sees the convergent flow between the Pacific and western Atlantic oceans. At the Atlantic a cyclonic flow and negative SLP is associated with a positive SST correlation, which suggest that the circulation as a response to SST anomaly is positively correlated with ACE-SON. A similar SST, SLP, and wind pattern is observed over the marginal seas of East Asia, but with much stronger negative correlation with SLP and smaller-scale circulation.

Figure 3(b) shows the lag correlation maps of ACE-SON and the large-scale variables in the preceding season JJA. A large region of positive correlation between ACE-SON and the SST over the west Pacific from 10°S to 40°N is evident. A weak anomalous anticyclone labelled as ***A*** is identified over the WNP with easterlies around 10°–20°N and 120°–140°E, westerlies around 30°–35°N and 130°–140°E, and to the south of the anticyclone showing anomalous southeasterlies round 5°N and 150°E. The anticyclone is collocated with the positive SST. Negative SLP correlation centred at (155°E, 40°N) is located to the north of the anticyclone. Another major area with negative SLP correlation is over the Southeast Asia and

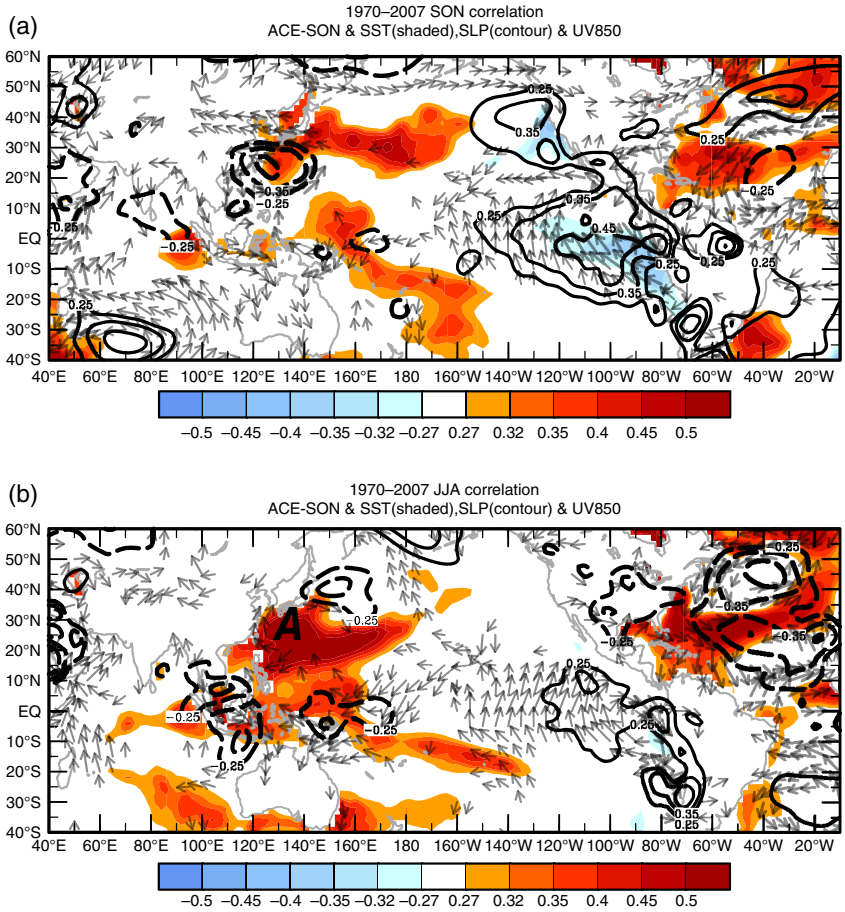

Figure 3. The linear correlation between ACE-SON and (a) SON and (b) JJA mean SST (shade), SLP (contours), and 850-hPa wind for the period of 1970–2007. The label 'A' marks the anomalous anticyclone near Taiwan and Japan. Only correlations significant at the level of 0.05 are presented. [Colour figure can be viewed at wileyonlinelibrary.com].

Indonesia maritime continent. The positive SST and the negative SLP correlations are collocated in the same region in the Tropics, while over the subtropics the positive SST and negative SLP are not collocated in the same region. It suggests that the negative SLP in the Tropics can be a response to the SST variations. Over the Atlantic, it shows a large area of significant positive SST associated with the cross-equatorial southerly winds over the eastern Pacific. Figure 3(a) shows an out-of-phase correlation relationship between North Atlantic and eastern South Pacific, which enhances the cross-equatorial southerly winds shown in the simultaneous correlation map of Figure 3(a). The positive SST correlation at WNP in Figure 3(a) is weaker than the correlation in Figure 3(b), while negative SLP correlation over Taiwan in Figure 3(a) is stronger than in Figure 3(b). The collocation of the negative SLP and positive SST suggests that late-season TC activity around Taiwan is more active when the subtropical high is weak and the west Pacific SST to the north of Papua New Guinea and Solomon Islands is warm.

To select the predictor candidates, we analysed the lag correlation between ACE-SON and the bi-monthly, tri-monthly mean anomalies and the changing tendency of two successive months of the large-scale variables, with the lag months from 1 to 6 months. Tables 2–4 summarize the selected candidates for the prediction models with the lead months from 0 to 2 months. The candidates are selected based on the seasonal correlation maps (Figures 3(a) and (b)) and the conceptual understanding of the physical linkage between the predictand and predictor fields. The potential predictors are further selected through a stepwise multivariate regression procedure available in MATLAB. The maximum number of predictors is limited to four to satisfy the 10% rule of the ratio of predictor and sample size. The predictors selected as a result of F-test with the F-value that can pass the 99% confidence interval of the regression model with the forecast lead times of 0–2 months are presented as follows.

3.2. Prediction models

3.2.1. Lead 0-month forecast

For lead 0 month, three predictors (SST_WNP_JA, SLP_AO_JJA, and SLP_WNP_8m7) are selected to form the following prediction model.

$$\begin{aligned}\text{ACE-SON} = {} & 0.49 \times (\text{SST\_WNP\_JA}) \\ & - 0.43 \times (\text{SLP\_AO\_JJA}) + 0.41 \\ & \times (\text{SLP\_WNP\_8m7}) + 1.6 \end{aligned} \quad (1)$$

Table 2. Predictor candidates used for lead 0 month forecast model development.

Predictor	Variables	Description
Lead 0 month		
SST_WNP_JA	SST	SST 2-month anomaly over WNP (15 –35 N, 120 –180 E)
SST_IO_JA	SST	SST 2-month anomaly over eastern equatorial Indian Ocean (10 S–10 N, 90 –130 E)
SST_WP_JA	SST	SST 2-month anomaly over western equatorial Pacific (5 S–10 N, 140 –170 E)
SST_AO_JA	SST	SST 2-month anomaly over North Atlantic Ocean (20 –35 N, 100 –30 W)
SST_WNP_JJA	SST	SST 3-month anomaly over WNP (10 –35 N, 120 –180 E)
SST_AO_JJA	SST	SST 3-month anomaly over North Atlantic Ocean (20 –30 N, 80 –30 W)
SLP_EP_JA	SLP	SLP 2-month anomaly over eastern equatorial Pacific (20 S–10 N, 130 –90 W)
SLP_AO_JA	SLP	SLP 2-month anomaly over North Atlantic Ocean (20 –30 N, 80 –30 W)
SLP_EP_JJA	SLP	SLP 3-month anomaly over eastern equatorial Pacific (120 –80 W, 10 S–10 N)
SLP_AO_JJA	SLP	SLP 3-month anomaly over North Atlantic Ocean (10 –50 N, 60 –20 W)
SST_EP_8m7	SST	SST tendency (August minus July) over equatorial eastern Pacific (10 S–10 N, 140 –90 W)
SLP_WNP_8m7	SLP	SLP tendency (August minus July) over WNP (20 –40 N, 170 E–160 W)
SLP_IO_8m7	SLP	SLP tendency (August minus July) over South Indian Ocean (10 –30 S, 110–140 E)
SLP_EP_8m6	SLP	SLP tendency (August minus June) over eastern equatorial Pacific (10 S–10 N, 120 –90 W)
SLP_WNP_8m6	SLP	SLP tendency (August minus June) over WNP Ocean (15 –30 N, 160 E–170 W)
SST_EP_8m6	SST	SST tendency (August minus June) over equatorial eastern Pacific (10 S–10 N, 120 –90 W)

The climatology used for anomaly calculation is the time mean of the training period of 1970–2007.

Table 3. Predictor candidates used for lead 1 month forecast model development.

Predictor	Variables	Description
Lead 1 month		
SST_WNP_JJ	SST	SST 2-month anomaly over WNP (15 –35 N, 130 –170E)
SST_EIOIS_JJ	SST	SST 2-month anomaly over eastern equatorial Indian Ocean and Indonesian Seas (10 S–10 N, 80 –130 E)
SST_AO_JJ	SST	SST 2-month anomaly over North Atlantic Ocean (20 –35 N, 80 –30 W)
SLP_SCSIO_JJ	SLP	SLP 2-month anomaly over southern SCS and equatorial eastern Indian Ocean (20 S–10 N, 100–125 E)
SLP_AO_JJ	SLP	SLP 2-month anomaly over North Atlantic Ocean (0 –30 N, 50 –20 W)
SST_WNP_MJJ	SST	SST 3-month anomaly over WNP (10 –30 N, 120 –170 E)
SST_WP_MJJ	SST	SST 3-month anomaly over western equator Pacific (10 S–10 N, 100 –150 E)
SST_AO_MJJ	SST	SST 3-month anomaly over North Atlantic Ocean (20 –30 N, 80 –30 W)
SLP_AO_MJJ	SLP	SLP 3-month anomaly over North Atlantic Ocean (10 –50 N, 60 –20 W)
SST_EP_7m6	SST	SST tendency (July minus June) over eastern South Pacific (30 –10 S, 120 –80 W)
SLP_WNP_7m6	SLP	SLP tendency (July minus July) over WNP (0 –30 N, 140 –180 E)

The climatology used for anomaly calculation is the time mean of the training period of 1970–2007.

The predictors in Equation (1) are presented in Figures 4(a)–(c). Figure 4(a) shows a large area of positive correlation of ACE-SON and the bi-monthly mean SST over WNP. The JA SST averaged over the area of 15°–35°N, 120°–180°E, named as SST_WNP_JA, is the first predictor in Equation (1). The positive SST correlation over the SST_WNP_JA area is associated with the southerly winds over the area centred at 15°N and 145°E and the easterly winds over the north Philippine Sea towards Taiwan. The second predictor SLP_AO_JJA is indicated by the negative correlation of ACE-SON and the JJA SLP over North Atlantic Ocean. The negative correlation is associated with cyclonic winds over mid-latitude (35°–50°N) and subtropical (10°–30°N) North Atlantic Ocean that is consistent with the SLP correlation. The third predictor marked in Figure 4(c) is SLP_WNP_8m7. The positive correlation with the July–August positive-tendency of the SLP over the central North Pacific northwest to the Hawaii islands is associated with high correlation of the strengthening of the southerly winds.

3.2.2. *Lead 1-month forecast*

For lead 1 month, it also turns out that three predictors (SST_WNP_MJJ, SLP_AO_MJJ, and SLP_SCSIO_JJ) are selected. The prediction model is:

$$\begin{aligned}\text{ACE-SON} = {} & 0.48 \times (\text{SST\_WNP\_MJJ}) \\ & - 0.57 \times (\text{SLP\_AO\_MJJ}) - 0.28 \\ & \times (\text{SLP\_SCSIO\_JJ}) + 1.6 \end{aligned} \quad (2)$$

The predictors in Equation (2) are presented in Figures 5(a) and (b). The correlation patterns in Figure 5(b) are similar to that in Figure 4(b). The first predictor SST_WNP_MJJ is marked over a large positive correlation area over WNP in Figure 5(a). The second predictor SLP_AO_MJJ is over the large area of negative correlation of SLP over North Atlantic Ocean. The negative correlation is associated with cyclonic winds over mid-latitude (35°–50°N) and subtropical (10°–30°N) North Atlantic Ocean, which shows consistent relationship with the SLP. The SLP and wind correlation patterns

Table 4. Predictor candidates used for lead 2 month forecast model development.

Predictor	Variables	Description
Lead 2 month		
SST_WNP_AM	SST	SST 2-month anomaly over WNP (15 –30 N, 125 –180 E)
SST_AO_AM	SST	SST 2-month anomaly over North Atlantic Ocean (20 –35 N, 80 –30 W)
SST_WNP_MJ	SST	SST 2-month anomaly over WNP (15 –35 N, 120 –180 E)
SST_AO_MJ	SST	SST 2-month anomaly over North Atlantic Ocean (20 –30 N, 80 –30 W)
SLP_AO_MJ	SLP	SLP 2-month anomaly over North Atlantic Ocean (20 –50 N, 60 –30 W)
SST_AO_MAM	SST	SST 3-month anomaly over North Atlantic Ocean (25 –35 N, 60 –30 W)
SST_WNP_AMJ	SST	SST 3-month anomaly over WNP (10 –30 N, 120 –160 E)
SST_AO_AMJ	SST	SST 3-month anomaly over North Atlantic Ocean (20 –35 N, 70 –20 W)
SST_EP_5m4	SST	SST tendency (May minus April) over eastern South Pacific (25 –10 S, 120 –75 W)
SLP_NP_5m4	SLP	SLP tendency (May minus April) over eastern North Pacific (15 –30 N, 180 –120 W)
SLP_EP_5m4	SLP	SLP tendency (May minus April) over eastern Pacific (20 S–15 N, 120 –80 W)
SLP_AO_5m4	SLP	SLP tendency (May minus April) over North Atlantic Ocean (10 –40 N, 60 –20 W)
SST_EP_6m4	SST	SST tendency (June minus April) over eastern South Pacific (20 S–0, 120 –80 W)
SLP_NP_6m4	SLP	SLP tendency (June minus April) over North Pacific (10 –25 N, 170 –130 W)
SLP_EP_6m5	SLP	SLP tendency (June minus May) over eastern South Pacific (30 S–0, 120 –80 W)
SLP_AO_6m5	SLP	SLP tendency (June minus May) over North Atlantic Ocean (10 –30 N, 80 –50 W)

The climatology used for anomaly calculation is the time mean of the training period of 1970–2007.

are consistent with the positive SST correlation that suggests the concurrent relationship between warm SST and the westerly and southerly associated with the cyclonic winds. The third predictor SLP_SCSIO_JJ is the negative correlation with the June and July mean SLP over the Southeast Asian maritime regions from the southern part of the SCS to the far eastern part of Indian Ocean (IO). The overall correlation patterns in Figure 5(b) suggest an enhanced Walker circulation with the enhanced convective centre over Southeast Asian seas and enhanced subsidence near the dateline.

3.2.3. Lead 2-month forecast

For lead 2 month, the selected predictors are SST_AO_MAM, SLP_EP_5m4, and SLP_NP_5m4. The prediction model is:

$$\begin{aligned}\text{ACE-SON} = {} & 0.67 \times (\text{SST\_AO\_MAM}) \\ & + 0.44 \times (\text{SLP\_EP\_5m4}) - 0.32 \\ & \times (\text{SLP\_NP\_5m4}) + 1.5 \end{aligned} \quad (3)$$

The predictors in Equation (3) are presented in Figures 6(a) and (b). The first predictor SST_AO_MAM is marked over the positive SST correlation over North Atlantic Ocean. The second predictor SLP_EP_5m4 is the negative correlation with the April–May SLP tendency over the eastern South Pacific. The third predictor is SLP_NP_5m4, the SLP tendency over the subtropical eastern North Pacific from April to May. Note that the SLP tendencies in the marked predictor areas in Figure 6(b) are opposite and these two predictors are uncorrelated as a requirement of the stepwise multivariate regression procedure. It suggests that when the mechanisms that separately generate a negative SLP tendency over the subtropical North Pacific and a positive tendency over the tropical eastern Pacific work together it can lead to a favourable condition to enhance the ACE-SON around Taiwan.

3.3. Forecast skill evaluation

The overall forecast ability of the multivariate regression model is evaluated using the standard leave-one-out cross validation procedure (Lu *et al.*, 2010). The predictor and predictand data set of T time points are divided into L segments. A model is then developed using the data of $L-1$ segments to predict ACE-SON in the remaining segment. This process is repeated by changing the segment that has been excluded from the model development. In addition to the leave-one-out, we also used leave-three-out, leave-seven-out, and leave-nine-out to evaluate the forecast skill, in which the prediction target is the second, fourth, fifth year of the removed consecutive 3, 7, and 9 years. All results are similar. Here we present the results for N predictions obtained from the leave-three-out evaluation (LTOCV) in Figures 7.

For the lead 0 month forecast, the correlation coefficient skill of the observed and LTOCV result reaches 0.70. For a sample size of 38, the critical value of 95% (99%) confidence level is 0.32 (0.41) when a two-tailed t-test is applied. Using the random number re-sampling technique to resample the data sets (Chu *et al.*, 2007), the 95% (99%) confidence level is 0.27 (0.38). Accordingly, the correlation coefficient (0.70) from the model developed in this study is deemed to be skilful relative to the benchmark random samples. The lead 1 and 2 months forecast results show similar skill examined through the LTOCV.

For the forecast period from 2008 to 2015, the correlations for lead 0, 1, and 2 months are 0.57, 0.6, and 0.47, respectively. The notable failed forecasts are the extremely high ACE year of 2008 and the low ACE years of 2011, 2012 for the lead 0 and lead 1, and the low ACE in 2014

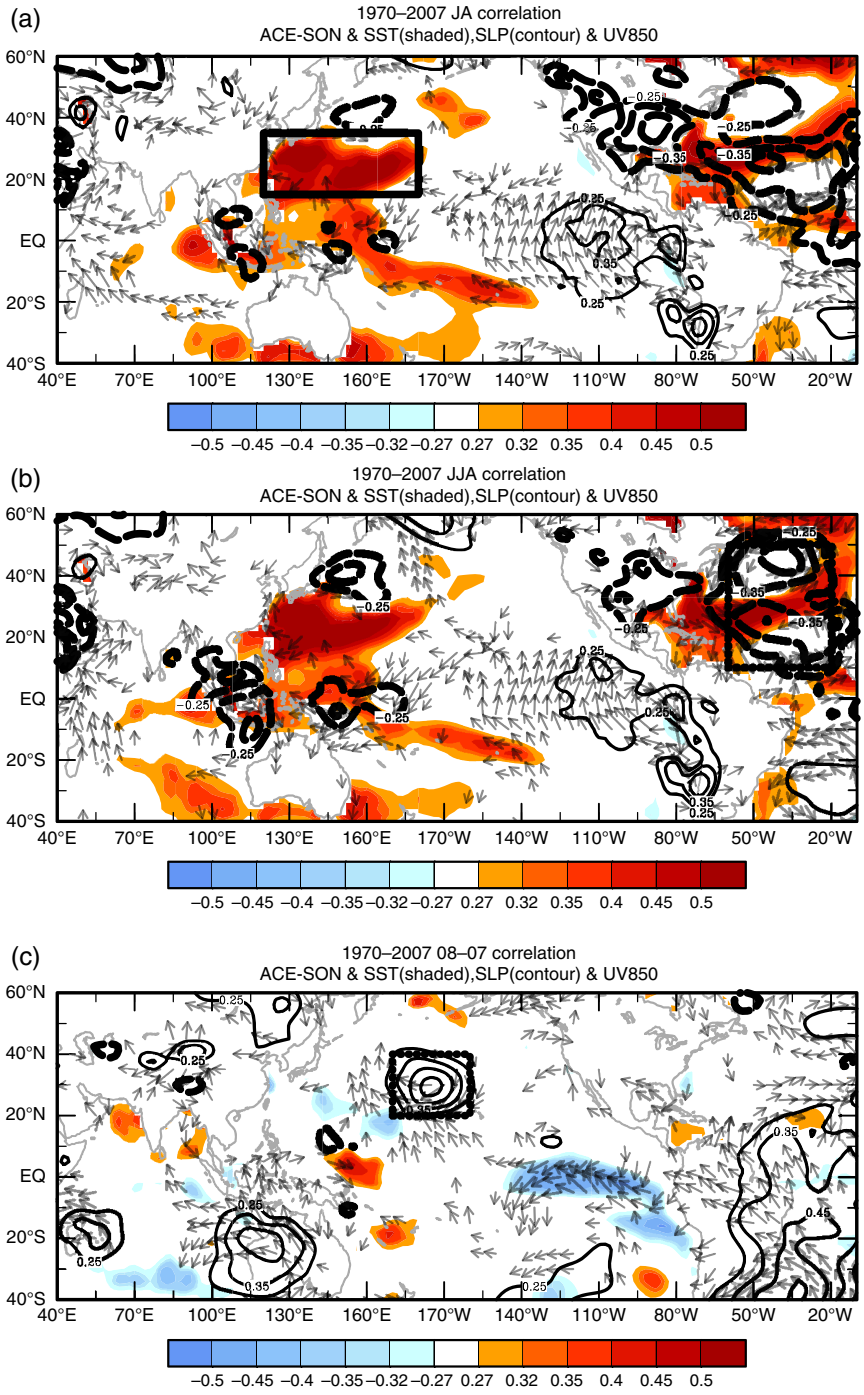

Figure 4. The same as in Figure 3 but for the correlation between ACE-SON and (a) July–August, (b) June–July–August, and (c) the 1-month tendency from July to August. Location of the selected predictor marked in solid (dashed) box for SST (SLP). [Colour figure can be viewed at wileyonlinelibrary.com].

for lead 2 forecasts. The failed cases will be discussed in later part of the article.

4. Predictability and attribution analysis

The sources of the predictability can be understood by contrasting the composite bi-monthly anomalies of SST, SLP, and UV850 for the correctly forecasted years, assumed that the signal to noise ratio is higher during these years. The selected are eight above-normal-ACE (1975, 1987, 1991, 1995, 1998, 2001, 2003, and 2007) and nine below-normal-ACE (1972, 1976, 1977, 1979, 1981, 1982, 1983, 1996, and 2002) years. Figures 8(a)–(h) show the composite maps from the winter-to-summer transitional months such as March, April, and May to the summer-to-winter transitional months such as September, October, and November. A clear contrast in the overall SST patterns is evident. The above-normal years (Figures 8(a)–(d)) saw warm SST anomalies over

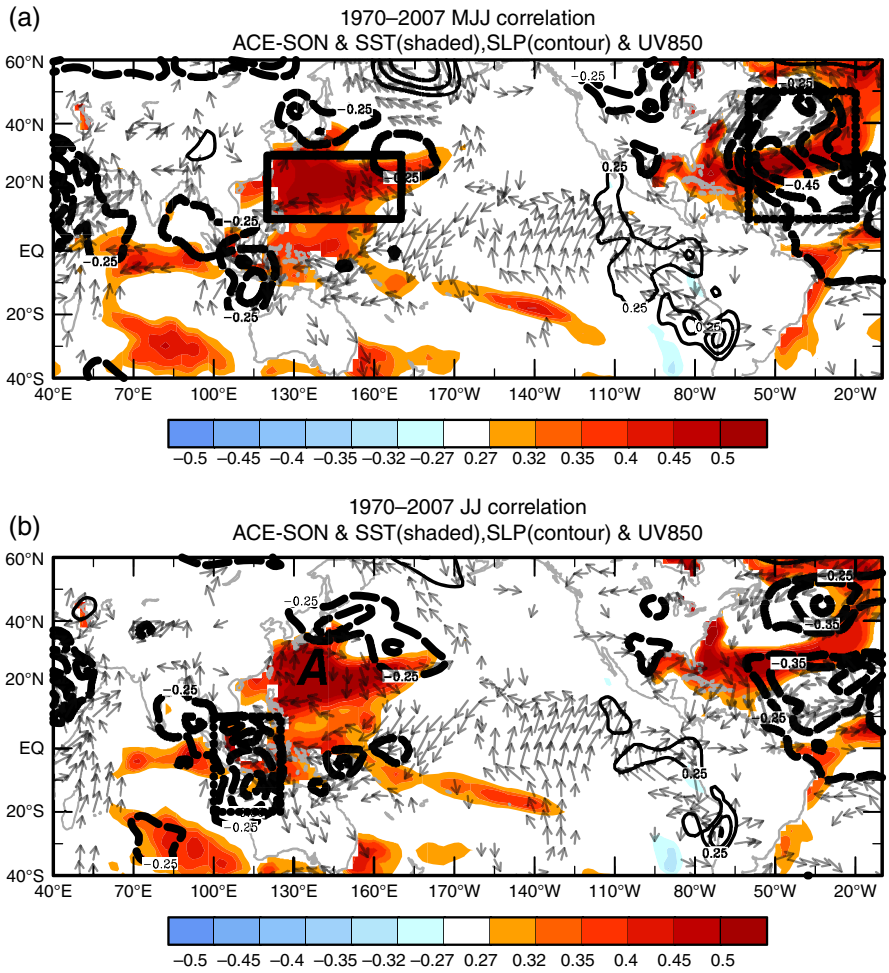

Figure 5. The same as in Figure 4 but for (a) May–June–July and (b) June–July means. [Colour figure can be viewed at wileyonlinelibrary.com].

the mid-latitude Atlantic Ocean and the Pacific western margins. Warm SST anomalies also appear over the IO during spring the summer season. The below-normal years (Figures 8(e)–(h)) saw cold SST anomalies over Atlantic and western Pacific oceans and warm SST anomalies over tropical eastern Pacific. Generally speaking, during the El Niño developing years when the SSTs over the marginal seas of the Indonesian and South Pacific islands are colder than normal, the ACE-SON tends to be below normal. When the west margins of the North Pacific have persistent warm SST anomalies from spring to summer and a synoptic-scale low pressure formed near Taiwan in late TC season, the ACE-SON tends to be above normal. The physical basis of the predictability is rooted in the El Niño-Southern Oscillation (ENSO) and North Atlantic SST influence on the west North Pacific TCs.

4.1. The ENSO influence

Wang and Chan (2002) documented the strong El Niño influence on WNP tropical storm activity. They found that ENSO affects TC genesis location. During El Niño summer and fall, the frequency of TC formation increases remarkably in the southeast quadrant (0°–17°N, 140°–180°E) and decreases in the northwest quadrant (17°–30°N, 120°–140°E). The July–September mean location of TC formation is 6° latitude lower, while that in October–December is 18° longitude eastwards in the strong warm *versus* strong cold years. ENSO influence shows strong phase lock effect with the annual cycle of the background monsoonal flow. The seasonal modulations of different impacts of the EP and central Pacific (CP) types of ENSO events (Ashok and Yamagata, 2009; Kao and Yu, 2009; Hu *et al.*, 2012; Yu *et al.*, 2012) on WNP TC has received much research interest (Hong *et al.*, 2011; Kim *et al.*, 2011; Ha *et al.*, 2013; Wang *et al.*, 2013a, 2013b, 2013c). Wang *et al.* (2013a) analysed the data that span the period of 1950–2009. They separated the TC seasons to early (April–June), peak (July–September), and late (October–December) seasons and found the sub-regional TC genesis, lifetime, and track density are sensitive to seasons and ENSO types. The track density and steering flow analysis (Wang *et al.*, 2013a, figure 12) supported the findings in the present article that the late-season TC activity around Taiwan is suppressed during the developing stage of the EP-type warm phase. The ACE-SON during EP-type warm years, such as 1972, 1976, 1982, and 1997 (Wang *et al.*, 2013a), is lower than normal (Figure 7), while the ACE-SON during the EP-type cold years, such as 1975, 1988, 2001, and 2008, is higher than normal (Figure 7). Wang *et al.* (2013a) only used the data

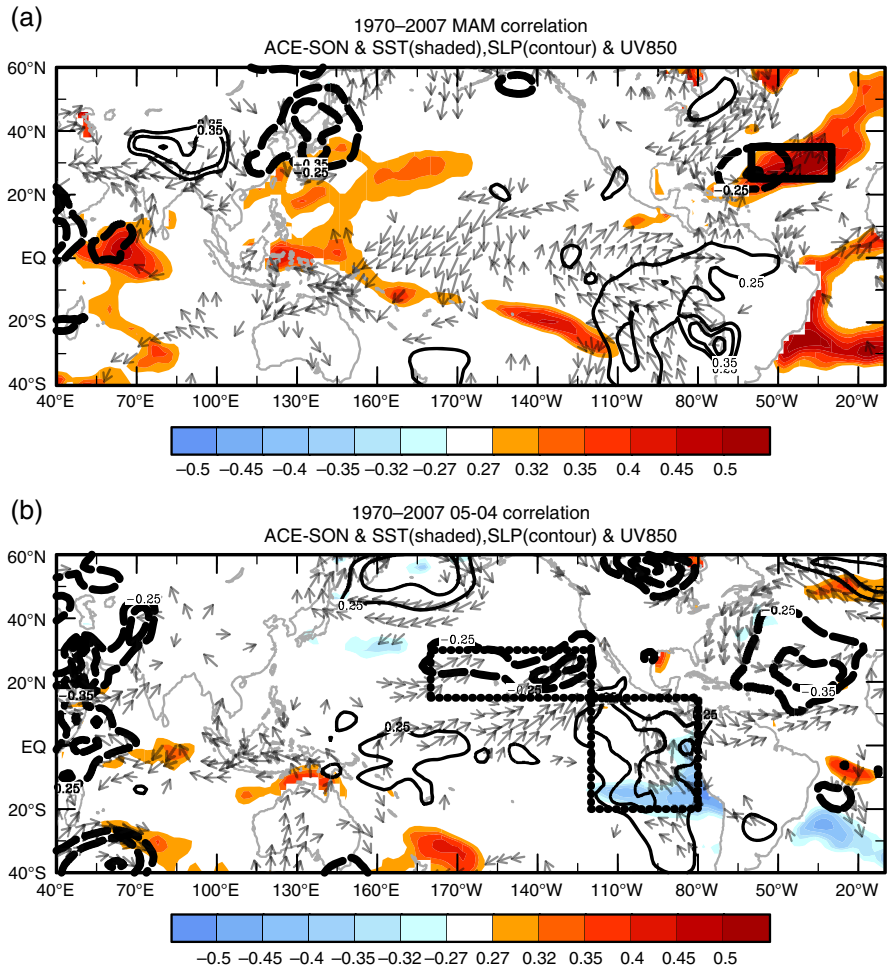

Figure 6. The same as in Figure 4 but for (a) March–April–May mean and (b) the 1-month tendency from April to May. [Colour figure can be viewed at wileyonlinelibrary.com].

up to 2009, the strong La Niña year 2010 is not in their list.

4.2. The North Atlantic influence

The influence of Atlantic SST on WNP TC genesis and tracks is another new research area actively studied. Huo *et al.* (2015) found remarkable negative correlation of WNP TC genesis frequency with the preceding boreal spring north tropical Atlantic (NTA) SST anomalies and proposed NTA SST as a predictor for the seasonal WNP TC activity. They pointed out that the predictability is rooted in the Matsuno-Gill-type Rossby wave atmospheric circulation anomaly during boreal spring that is excited by the intensified Atlantic to Pacific teleconnection (Ham *et al.*, 2013) and sustained through the local air–sea coupling and instability that lasts throughout the typhoon season. Ham *et al.* (2013) pointed out that NTA SST and the Atlantic Niño during the boreal spring are two independent predictors for predicting the development of ENSO events in the following season. The NTA sea surface cooling during FMA leads the CP warming in the following winter season, while the tropical eastern Atlantic cooling in JJA leads the eastern Pacific warming in the following winter. Yu *et al.* (2015) found the significant simultaneous negative relationship between the TC genesis number during JASO over the WNP and the SST anomaly in the tropical North Atlantic (TNA). Cold TNA SST can enhance the WNP monsoon trough through strengthening the low-level westerly winds over the tropical IO in boreal summer. The intensified low-level westerly winds of the IO can enhance the surface evaporation and cool the *in situ* SST. It subsequently suppresses the convection of the IO and further enhances the low-level westerly winds from the IO to WNP, hence intensifying the WNP monsoon trough. This relationship is consistent with the IO SST influence to the trade winds in the WNP proposed by Luo *et al.* (2012). Zhang *et al.* (2017) found the Atlantic meridional mode (AMM) can modulate the peak season (June–November) WNP TC activity by influencing the zonal vertical wind shear (ZVWS) caused by AMM-induced changes to the Walker circulation. When the NAT is warmer than usual (positive AMM phase), it induces strong descending flow in the tropical and CP (140°E–100°W), so that the regional Walker cell with the anomalously ascending branch in 120°–150°E is intensified. The intensified Walker cell is responsible for the suppressed (enhanced) TC genesis in the eastern (western, west to 140°E) part of the WNP by strengthening (weakening) ZVWS.

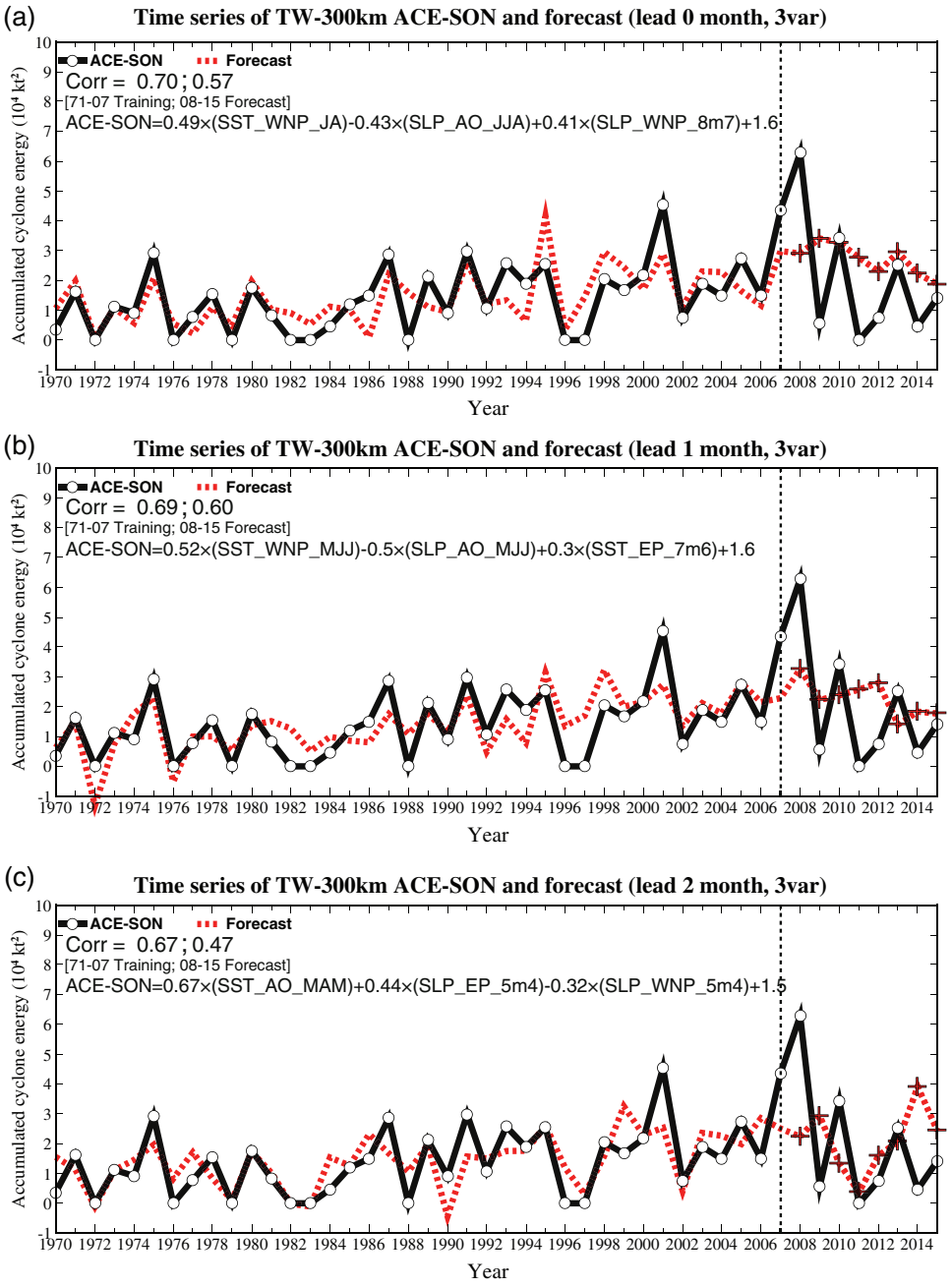

Figure 7. The time series of the LTOCV result of the forecast ACE-SON (dashed line) compared with the observation (solid line) during the period from 1970 to 2015 for lead (a) 0, (b) 1, (c) 2 months forecast models and the forecast equations. A description of the predictors is summarized in Tables 2–4. On the upper left corner are the correlation (Corr) between the observation and forecast time series during the LTOCV period (1970–2007) followed by the correlation during the forecast period (2008–2015). The forecast results marked by '+'. [Colour figure can be viewed at wileyonlinelibrary.com].

In the present study, the spring and summer NTA SST and North Atlantic SLP are identified as the predictors of ACE-SON variation. The physical explanation is in line with the AMM influence on the Walker circulation described by Zhang *et al.* (2017). We noticed that the correlation patterns of NTA SST (Figure 3(a)) resemble the NTA SST pattern of the AMM shown by Zhang *et al.* (2017, figure 1). The composite 850-hPa winds for the above-normal years (Figures 8(a)–(d)) show enhanced easterlies to the east of 150°E and westerlies to the west of 160°W; hence, the anomalous zonal winds are with a divergence centre near the date line, which is consistent with the aforementioned AMM influence on the Walker circulation. The opposite zonal wind anomalies are observed in the composite 850-hPa winds for the below-normal years (Figures 8(e)–(h)). The anomalous low-level divergence (convergence) in JJA induces the warm (cold) SST in the Pacific Ocean western margins during the following SON season and anomalous low-pressure and cyclonic (anticyclonic) flow near Taiwan, therefore resulting in above (below) normal TC activity in the region.

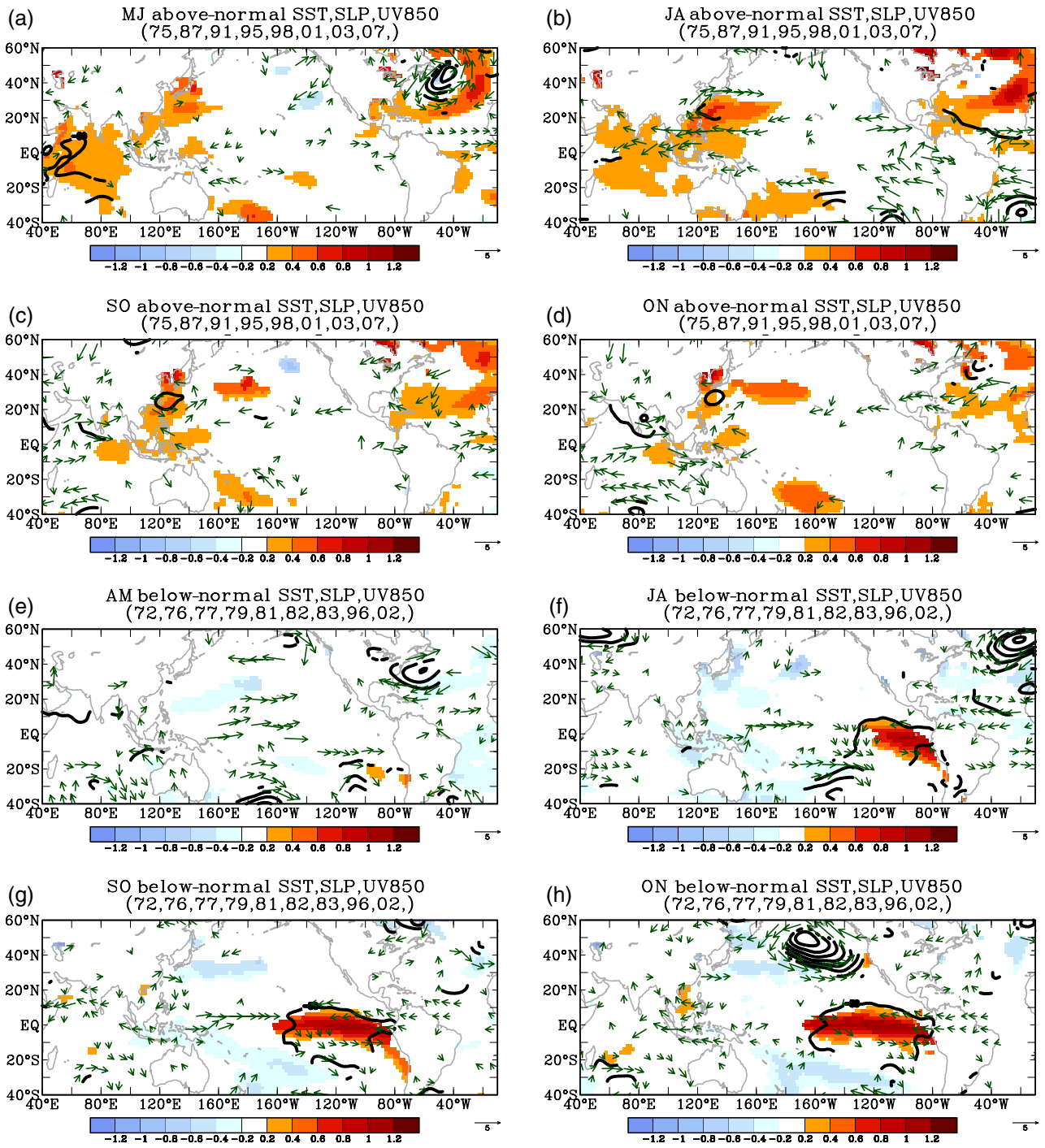

Figure 8. The bi-monthly mean large-scale parameters of SST (shade), SLP (contours), and 850-hPa wind anomalies composite for the ACE-SON above-normal years (1975, 1987, 1991, 1995, 1998, 2001, 2003, and 2007) for the months of (a) May–June, (b) July–August, (c) September–October, and (d) October–November, and below-normal years (1972, 1976, 1977, 1981, 1982, 1983, 1996, and 2002) for the months of (e) April–May, (f) JA, (g) SO, and (h) ON. Only correlations significant at the level of 0.05 are presented. [Colour figure can be viewed at wileyonlinelibrary.com].

5. Discussion and application

We have presented the model building and skill evaluation procedure and the result of three statistical models for predicting ACE-SON in 0, 1, and 2 months ahead. The leave-one-out, leave-seven-out, and leave-nine-out cross-validation tests using the 38 years of data from 1970 to 2007 show substantial forecast skill of three models. The forecast experiment for the period of 2008–2015 that mimics the real forecast also supports the skill of the forecast model.

The predictability of these models is rooted in the teleconnection of Atlantic–Pacific–Southeast Asia marginal seas. If from JJA to SON the SST in the Pacific western margins is persistently warmer (colder) than usual, then

the ACE-SON tends to be higher (lower) than normal. For ACE-SON above-normal years, the anomalous cyclonic low-level winds and below-normal SLP observed in the correlation (Figure 3(a)) and composite (Figures 8(c) and (d)) maps resemble the strong monsoon gyre (Molinari and Vollaro, 2017). For ACE-SON below-normal years, the anomalous anticyclonic low-level winds observed over the SCS and the Philippine Sea in the correlation (Figure 3(a)) and composite maps (Figures 8(g) and (h)) resemble the weak monsoon trough (Molinari and Vollaro, 2013).

The geographic location of Taiwan makes the late TC season ACE forecast sensitive to tropical and mid-latitude SST anomalies. It is interesting to note that the monsoon-gyre-like anticyclone is centred near 25°N (Figure 8(c)), while the monsoon-trough-like anticyclone is centred near 15°N (Figure 8(g)). To associate the monsoonal synoptic features with TC activity, we present the composite SON TC density maps for high and low ACE-SON years in Figures 9(a) and (b). For the above-normal ACE-SON years, Figure 9(a) shows high TC density centres around Taiwan, the SCS, and the Philippine Sea. However, for below-normal ACE-SON years, Figure 9(b) shows that major high TC density centres are located within the monsoon trough that extends from the SCS through the Philippine Sea to Micronesia islands. Figure 9(b) also shows more TC genesis to the north of the monsoon trough when ACE-SON is below normal. The TC density difference between the above-normal and below-normal years (Figure 9(c)) shows the negative string oriented in northwest–southeast direction from Hainan Island to the Luzon Sea and the Philippine Sea to the Pacific islands centred around Guam (13°N, 144°E). However, to the north and south of the negative string are the positive strings to the north and south. The result suggests that the late-season TC activity in west margins of the Pacific Ocean is sensitive to the TC tracks modulated by the large-scale environment.

The predictors used in the present models can be applied to forecast the ACE of the southeast China coastal regions, marked by the two rectangular boxes in Figure 9(c), with 0 and 1 month leads. The northern box is bounded by 115°–119°E and 22°–25.5°N, and the southern box is bounded by 117.5°–122°E, 25.5°–30°N. The SON ACE within these two box areas is termed as SEC to represent southeast China ACE. Figures 10(a) and (b) show the observed and forecast SEC during the training and forecast period with the 0 and 1 month leads. The correlation coefficient skill of the observed and LTOCV for the 0 (1) month lead is 0.35 (0.41), significant at the 95% confidence level. A noteworthy feature in Figure 10 is a shift of the SEC variability from the quiet period of 1970–1989 to a violent regime with large interannual variation since 1990. The shift can be related to the westwards extension of the western Pacific subtropical high (Zhou *et al.*, 2009). However, it is noted that the long-term variation in the seasonal typhoon ACE in the WNP region is drastically different from that in a limited area. The former shows evident multi-decadal decline of the TC activity since 1990

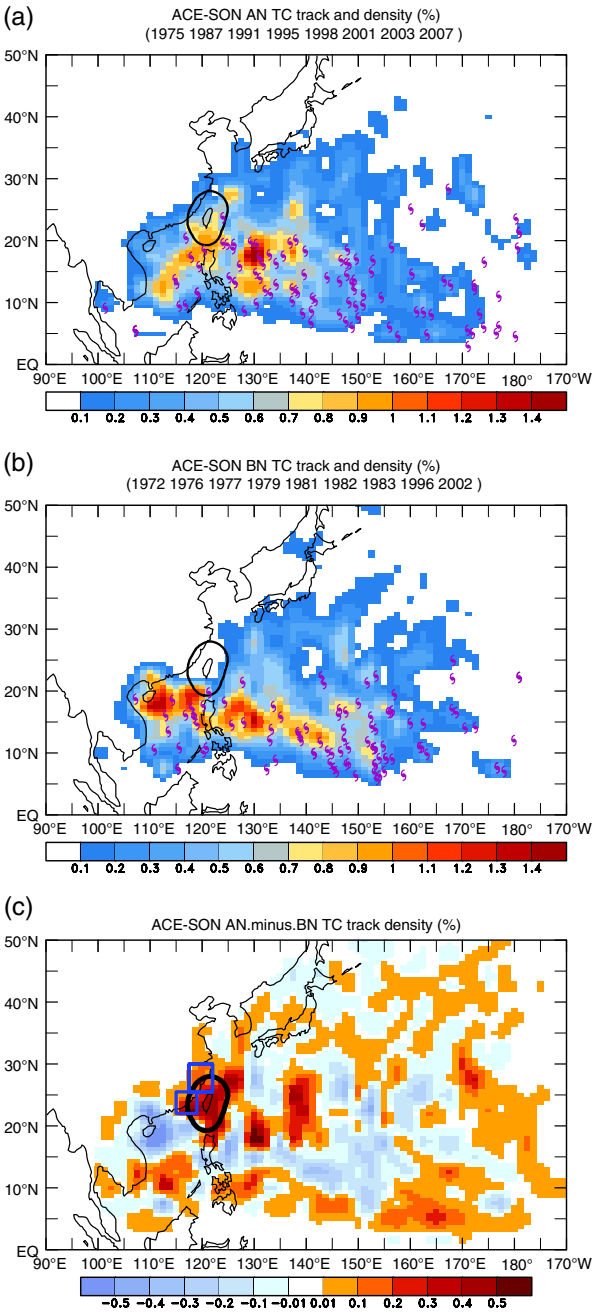

Figure 9. The composite TC track density and tracks for (a) the ACE-SON above-normal years, (b) the ACE-SON below-normal years, and (c) the difference between the ACE-SON above and below-normal years. The two rectangular boxes near Taiwan mark the area for the typhoon ACE of the southeast China region. [Colour figure can be viewed at wileyonlinelibrary.com].

(Maue, 2011; Liu and Chan, 2013; Wang *et al.*, 2013a; Hsu *et al.*, 2014; Lin and Chan, 2015), while the later, particularly in Taiwan area (Figure 7), shows clear interannual fluctuations. Detailed discussion is beyond this article and will be published separately.

The ACE-SON forecast can also be applied to seasonal rainfall outlook. Although the relationship of typhoon rainfall and intensity is weak for an individual typhoon, the relationship of seasonal accumulated rainfall over Taiwan and the accumulated cyclone kinetic energy is quite good.

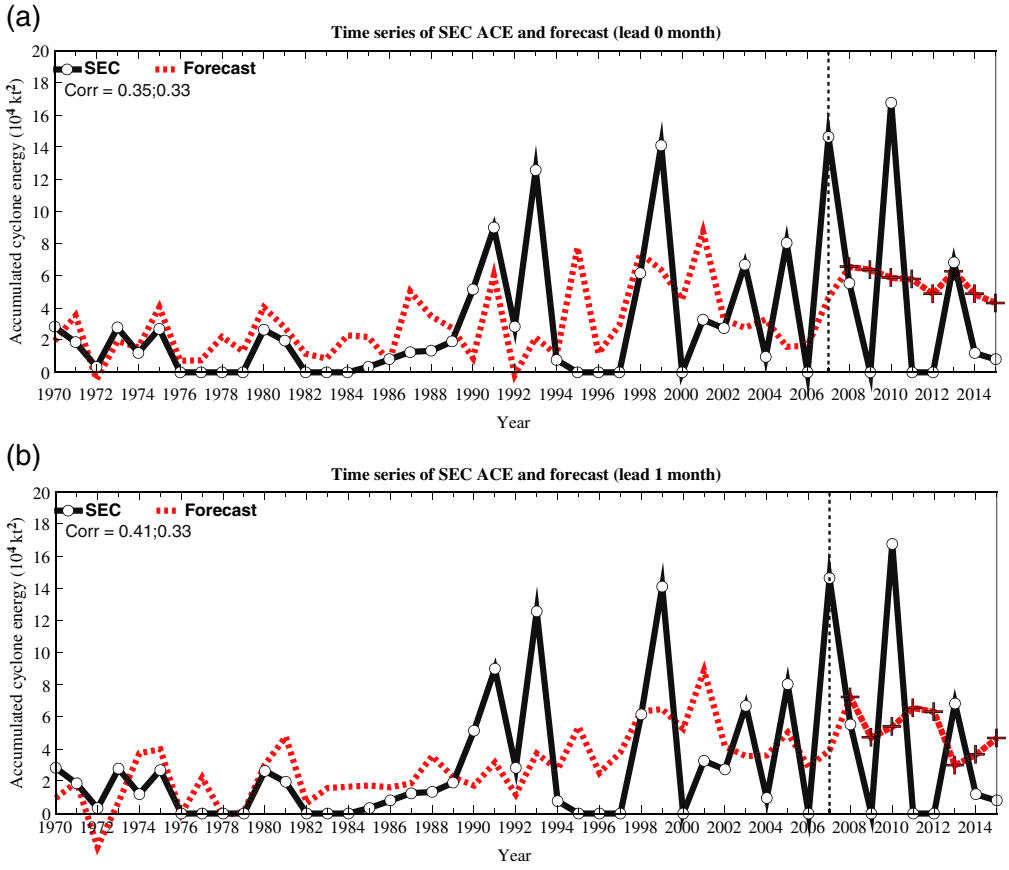

Figure 10. The same as in Figure 7 but for the SEC region, marked as two rectangular boxes in Figure 9, for the (a) 0 and (b) 1 month lead forecasts. [Colour figure can be viewed at wileyonlinelibrary.com].

The SON rainfall totals measured at six stations to the west of Taiwan central mountain range has the correlation with ACE-SON as high as 0.71. If we use the ACE-SON tercile-category forecast for rainfall outlook, the GSS scores reach 0.26, 0.21, and 0.26 for lead 0, 1, and 2 months of the forecasts. For example, in the lead 0 case among the 15 outlooks of the below (above) normal SON rain only 2 years turned out to be above (below) normal. Because from December to April is the dry months of west Taiwan, the SON rainfall outlook is a wanted information to water resource managers.

The ACE-SON variability is highly influenced by the frequency of intense TCs within the 300-km boundary. The outstanding ACE-SON in 2001, 2007, and 2008 are caused by unusually frequent strong TCs. Although the wind speed estimated by different centres is different and stronger TC has larger difference, the difference disappears when the ACE-SON is classified to tercile categories. In 2008 three typhoons, two category 4 and one category 5, entered into the 300-km boundary surrounding Taiwan and one made landfall. This is why the ACE-SON time series shows an outstanding peak in 2008. Although the forecast ACE-SON is above normal, the model is not able to predict such an unusual situation of the successive attack of three strong typhoons.

Comprehensive monitoring and analysing climate variability on subseasonal to seasonal time scales is of great importance in real time. For example, the notable failed cases of 2011, 2012 for the lead 0 and lead 1 forecasts and 2014 for lead 2 forecast can be attributed to the influence of well-below-normal global TC activity and strong MJO in 2011, and the never developed El Nino in 2014 is not considered in the models. The year of 2011 is characterized by two distinct La Niña episodes sandwiched around a period of ENSO neutral conditions from April to August (Diamond, 2012). The lead 2 model has two predictors of the SLP tendency during the spring season over the North Pacific and EP (Figure 6) that actually captured the atmospheric features during the decaying phase instead of the developing phase of a La Niña event and then produced a forecast of below-normal ACE-SON. The predictors of lead 1 and lead 0 models captured some part of the SST and SLP characteristics over west Pacific and Southeast Asia during a La Niña year, therefore overly estimated the ACE-SON. In other words, the failure of the prediction can be attributed to the un-typical relationship between WNP TC activity in 2011 compared with the La Niña years with similar evolution patterns on which the predictability is based. 2011 is also characterized by a dramatic change in WNP TC activity from September to October (Camargo, 2012). The WNP ACE in September was above normal but in October it was close to the historical minimum for that month. The abrupt change may be resulted from the combined effect of a strong MJO event with particularly intense

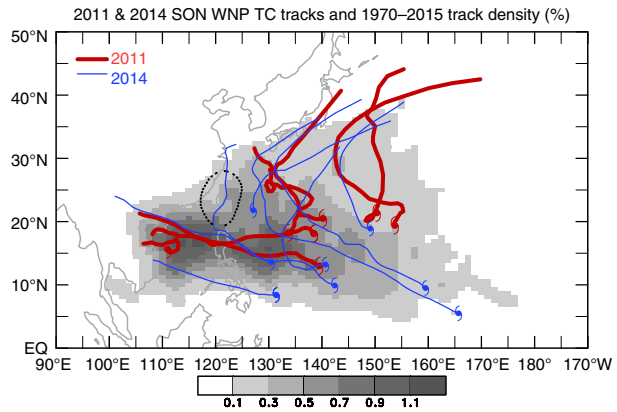

Figure 11. The same as in Figure 9 but for 2011 (thick tracks) and 2014 (thin tracks). The background grey shade is the 46-year (1970–2015) ACE-SON climatology. [Colour figure can be viewed at wileyonlinelibrary.com].

convection over the IO during late October/early November (Gottschalck and Bell, 2012) and the strengthening La Niña. In contrast to 2011, 2014 was largely ENSO-neutral, although there were borderline La Niña conditions in early 2014 and borderline El Niño conditions in late 2014 (Diamond, 2012). No clear El Niño like atmospheric response to the warm equatorial Pacific SST was detected. The failure of lead 2 model in 2014 can be attributed to a strong precursor signal for a developing La Niña, captured by the two predictors of the SLP tendency during the spring season over the North Pacific and EP (Figure 6), which failed to be realized. The TC geographical distribution in 2011and 2014 (Figure 11) indeed reflects the ENSO influence such as less active TC activity in the southeast quadrant (0°–17°N, 140°–180°E) in 2011 the La Niña year, while more active TC activity in the southeast quadrant in 2014, the borderline El Niño year. However, the influence of well-below-normal global TC activity and strong MJO in 2011 and the never developed El Nino in 2014 is not considered in the forecast models presented in this article. Therefore, when applying the prediction model to real-time forecast, the decision needs the support from real-time climate monitoring and analysis.

There are several directions for the future work. For example, the forecast skill of the predictors presented in this study can be evaluated using seasonal forecast models (Wang *et al.*, 2005, 2015) such as the North American multimodel ensemble (NMME) data sets (Kirtman *et al.*, 2014; Ma *et al.*, 2017). The predictors of the empirical forecast models can be replaced by the variables forecasted by the skilful dynamical models to increase the forecast lead time. In addition, new predictors such as the subsurface seawater temperature (Jin *et al.*, 2014; Lin *et al.*, 2014; Zheng *et al.*, 2015) in seasonal climate forecast models should be explored and new statistical forecast models can be developed. Finally, this study used the NCEP-NCAR reanalysis and ERSST data sets for identifying the predictors for a practical reason of rapid update of the data so that it can be used for real-time operational applications. Different reanalysis data sets (e.g. Dee *et al.*, 2011) should be explored in the future when the real-time data can be freely accessed.

Acknowledgements

This work was supported by the Central Weather Bureau of Taiwan under Toward Smart Weather Information Application and Service Project. This is the ESMC publication number 183.

References

Ashok K, Yamagata T. 2009. Climate change: the El Niño with a difference. *Nature* **461**: 481–484. https://doi.org/10.1038/461481a.

Bell GD, Halpert MS, Schnell RC, Higgins RW, Lawrimore J, Kousky VE, Tinker R, Thiaw W, Chelliah M, Artusa A. 2000. The 1999 North Atlantic and eastern North Pacific hurricane seasons. *Bull. Am. Meteorol. Soc.* **81**(6, Suppl): S19–S22.

Camargo SJ. 2012. Western North Pacific Basin. *Bull. Am. Meteorol. Soc.* **93**(7, Suppl): S107–S109.

Chu PS, Zhao X, Lee CT, MM L. 2007. Climate prediction of Taiwan cyclone activity in the vicinity of Taiwan using the multivariate least absolute deviation regression method. *Terr. Atmos. Ocean. Sci.* **13**: 469–498.

Dee DP, Uppala SM, Simmons AJ, Berrisford P, Poli P, Kobayashi S, Andrae U, Balmaseda MA, Balsamo G, Bauer P, Bechtold P, Beljaars ACM, van de Berg L, Bidlot J, Bormann N, Delsol C, Dragani R, Fuentes M, Geer AJ, Haimberger L, Healy SB, Hersbach H, Hólm EV, Isaksen L, Kållberg P, Köhler M, Matricardi M, McNally AP, Monge-Sanz BM, Morcrette JJ, Park BK, Peubey C, de Rosnay P, Tavolato C, Thépaut JN, Vitart F. 2011. The ERA-Interim reanalysis: Configuration and performance of the data assimilation system. *Q. J. R. Meteorol. Soc.* **137**: 553–597.

Diamond HJ (ed). 2012. The tropics. *Bull. Am. Meteorol. Soc.* **93**(7, Suppl): S93–S126.

Gottschalck J, Bell GD. 2012. Tropical intraseasonl activity. *Bull. Am. Meteorol. Soc.* **93**(7, Suppl): S97–S98.

Ha Y, Zhong Z, Yang X, Sun Y. 2013. Different Pacific Ocean warming decaying types and Northwest Pacific tropical cyclone activity. *J. Clim.* **15**: 8979–8994. https://doi.org/10.1175/JCLI-D-13-00097.1.

Ham YY, Kug JS, Park JY, Jin FF. 2013. Two distinct roles of Atlantic SSTs in ENSO variability: north tropical Atlantic SST and Atlantic Niño. *Geophys. Res. Lett.* **40**: 4012–4017.

Hong CC, Li YH, Li T, Lee MY. 2011. Impacts of central Pacific and eastern Pacific El Niños on tropical cyclone tracks over the western North Pacific. *Geophys. Res. Lett.* **38**: L16712. https://doi.org/10.1029/2011GL048821.

Hsu PC, Chu PS, Murakami H, Zhao X. 2014. An abrupt decrease in the late season typhoon activity over the western North Pacific. *J. Clim.* **27**: 4296–4312.

Hu ZZ, Kumar A, Jha B, Wang W, Huang B. 2012. An analysis of warm pool and cold tongue El Niños: Air–sea coupling processes, global influences, and recent trends. *Clim. Dyn.* **38**: 2017–2035. https://doi.org/10.1007/s00382-011-1224-9.

Huo L, Guo P, Hameed SN, Jin D. 2015. The role of tropical Atlantic SST anomalies in modulating western North Pacific tropical cyclone genesis. *Geophys. Res. Lett.* **42**: 2378–2484.

Jin FF, Boucharel J, Lin II. 2014. Eastern Pacific tropical cyclones intensified by El Nino delivery of subsurface ocean heat. *Nature* **516**: 82–85. https://doi.org/10.1038/nature13958.

Kalnay E, Kanamitsu M, Kistler R, Collins W, Deaven D, Gandin L, Iredell M, Saha S, White G, Woollen J, Zhu Y, Leetmaa A, Reynolds R, Chelliah M, Ebisuzaki W, Higgins W, Janowiak J, Mo KC, Ropelewski C, Wang J, Jenne R, Joseph D. 1996. The NCEP/NCAR 40-year reanalysis project. *Bull. Am. Meteorol. Soc.* **77**: 437–471.

Kao HY, Yu JY. 2009. Contrasting eastern Pacific and central Pacific types of ENSO. *J. Clim.* **22**: 615–631.

Kim HM, Webster PJ, Curry JA. 2011. Modulation of North Pacific tropical cyclone activity by three phases of ENSO. *J. Clim.* **24**: 1839–1849. https://doi.org/10.1175/2010JCLI3939.1.

Kirtman BP, Min D, Infanti JM, Kinter III JL, Paolino DA, Zhang Q, van den Dool H, Saha S, Mendez MP, Becker E, Peng P, Tripp P, Huang J, DeWitt DG, Tippett MK, Barnston AG, Li S, Rosati A, Schubert

SD, Rienecker M, Suarez M, Li ZE, Marshak J, Lim YK, Tribbia J, Pegion K, Merryfield WJ, Denis B, Wood EF. 2014. The North American multimodel ensemble: phase-1 seasonal-to-interannual prediction; phase-2 toward developing intraseasonal prediction. *Bull. Am. Meteorol. Soc.* **95**: 585–601. https://doi.org/10.1175/BAMS-D-12-00050.1.

Lin II, Chan JCL. 2015. Recent decrease in typhoon destructive potential and global warming implications. *Nat. Commun.* **6**: 7182. https://doi.org/10.1038/ncomms8182.

Lin II, Pun IF, Lien CC. 2014. 'Category-6' supertyphoon Haiyan in global warming hiatus: contribution from subsurface ocean warming. *Geophys. Res. Lett.* **41**: 8547–8553.

Liu KS, Chan JCL. 2013. Inactive period of western North Pacific tropical cyclone activity in 1998-2011. *J. Clim.* **26**: 2614–2630.

Luo JJ, Sasaki W, Masumoto Y. 2012. Indian Ocean warming modulates Pacific climate change. *Proc. Natl Acad. Sci. U.S.A.* **109**: 18701–18706.

Ma J, Xie SP, Xu H. 2017. Intermember variability of the summer northwest Pacific subtropical anticyclone in the ensemble forecast. *J. Clim.* **30**(10): 3927–3941.

Maue RN. 2011. Recent historically low global tropical cyclone activity. *Geophys. Res. Lett.* **38**: L14803. https://doi.org/10.1029/2011GL047711.

Lu MM, Chu PS, Lin YC. 2010. Seasonal prediction of tropical cyclone activity in the vicinity of Taiwan using the Bayesian multivariate regression method. *Weather Forecast.* **25**: 1780–1759.

Lu MM, Lee CT, Wang B. 2013. Seasonal prediction of accumulated tropical cyclone kinetic energy around Taiwan and the sources of the predictability. *Int. J. Climatol.* **33**: 2846–2854. https://doi.org/10.1002/joc.3634.

Molinari J, Vollaro D. 2013. What percentage of western North Pacific tropical cyclones form within the monsoon trough? *Mon. Weather Rev.* **141**: 499–505. https://doi.org/10.1175/MWR-D-12-00165.1.

Molinari J, Vollaro D. 2017. Monsoon gyres of the northwest Pacific: Influences of ENSO, the MJO, and the Pacific–Japan Pattern. *J. Clim.* **30**: 1765–1777.

Wang B, Chan JCL. 2002. How strong ENSO events affect tropical storm activity over the western North Pacific. *J. Clim.* **15**: 1643–1658.

Wang B, Ding Q, Fu X, Kang IS, Jin K, Shukla J, Doblas-Reyes F. 2005. Fundamental challenge in simulation and prediction of summer monsoon rainfall. *Geophys. Res. Lett.* **32**: L15711. https://doi.org/10.1029/2005GL022734.

Wang C, Li C, Mu M, Duan W. 2013a. Seasonal modulations of different impacts of two types of ENSO events on tropical cyclone activity in the western North Pacific. *Climate Dyn.* **40**: 2887–2902. https://doi.org/10.1007/s00382-012-1434-9.

Wang B, Liu J, Kim HJ, Webster PJ, Yim SY, Xiang B. 2013b. Northern Hemisphere summer monsoon intensified by mega-El Niño/southern oscillation and Atlantic multidecadal oscillation. *Proc. Natl Acad. Sci. U.S.A.* **110**: 5347–5352.

Wang B, Xiang B, Lee JY. 2013c. Subtropical high predictability establishes a promising way for monsoon and tropical storm predictions. *Proc. Natl Acad. Sci. U.S.A.* **110**: 2718–2722.

Wang B, Xiang B, Li J, Webster PJ, Rajeevan MN, Liu J, Ha KJ. 2015. Rethinking Indian monsoon rainfall prediction in the context of recent global warming. *Nat. Commun.* **6**: 7154. https://doi.org/10.1038/ncomms8154.

Yu JY, Chou C, Chiu PG. 2009. A revised accumulated cyclone energy index. *Geophys. Res. Lett.* **36**: L14710. https://doi.org/10.1029/2009GL039254.

Yu JY, Lu MM, Kim ST. 2012. A change in the relationship between tropical central Pacific SST variability and the extratropical atmosphere around 1990. *Environ. Res. Lett.* **7**(3): 034025. https://doi.org/10.1088/1748-9326/7/3/034025.

Yu J, Li T, Tan Z, Zhu Z. 2015. Effects of tropical North Atlantic SST on tropical cyclone genesis in the western North Pacific. *Clim. Dyn.* **46**: 865–877.

Zhang W, Vecchi GA, Villarini G, Murakami H, Rosati A, Yang X, Jia L, Zeng F. 2017. Modulation of western North Pacific tropical cyclone activity by the Atlantic meridional mode. *Clim. Dyn.* **48**: 631–647. https://doi.org/10.1007/s00382-016-3099-2.

Zheng ZW, Lin II, Wang B, Huang HC, Chen CH. 2015. A long neglected damper in the El Niño-typhoon relationship: a 'Gaia-like' process. *Sci. Rep.* **5**: 11103. https://doi.org/10.1038/srep11103.

Zhou T, Yu R, Zhang J, Drange H, Cassou C, Deser C, Hodson DLR, Sanchez-Gomez E, Li J, Keenlyside N, Xin X, Okumura Y. 2009. Why the western Pacific subtropical high has extended westward since the late 1970. *J. Clim.* **22**: 2199–2215.